

## Prepulse effects on the interaction of intense femtosecond laser pulses with high-Z solids

Alexei Zhidkov, Akira Sasaki, Takayuki Utsumi, and Ichirou Fukumoto  
Advanced Photon Research Center, JAERI, 25-1, Mii-minami-machi, Neyagawa, Osaka 572-0019, Japan

Toshiki Tajima  
Lawrence Livermore National Laboratory, L-441, Livermore, California 94551

Fumikazu Saito, Yoichiro Hironaka, Kazutaka G. Nakamura, and Ken-ichi Kondo  
Materials and Structures Laboratory, Tokyo Institute of Technology, 4259 Nagatsuta, Midori, Yokohama, Kanagawa 226-8503, Japan

Masatake Yoshida  
National Institute of Material and Chemical Research, 1-1 Higashi, Tsukuba, Ibaraki 305-8565, Japan  
(Received 23 May 2000)

$K\alpha$  emission of high-Z solid targets irradiated by an intense, short ( $<100$  fs) laser pulse in the 10 keV region is shown to be sensitive to the electron energy cutoff, which is strongly dependent on the density gradient of the plasma corona formed by a long prepulse. The absorption rate of short laser pulses, the hot electron distribution, and x-ray emission from a Cu slab target are studied via a hybrid model, which combines the hydrodynamics, collisional particle-in-cell, and Monte Carlo simulation techniques, and via a direct spectroscopic measurement. An absorption mechanism originating from the interaction of the laser pulse with plasma waves is found to increase the absorption rate by over 30% even for a very short,  $s$ -polarized laser pulse. Calculated and measured x-ray spectra are in good agreement, confirming the electron energy cutoff.

PACS number(s): 52.40.Nk

### I. INTRODUCTION

Solids of high-Z matter irradiated by an intense short pulse laser constitute a high-brightness source of  $K\alpha$  emission [1–8]. With an increase in laser intensity, one expects efficient x-ray emission in the 10–100 keV range with a pulse duration shorter than 10 ps. This short incoherent x-ray emission may be used for time-resolved measurements in various medical and material processing applications [6].

Hot electrons produced during the interaction of a laser pulse with plasmas are the pumping source for  $K\alpha$  emission. On the other hand, a part of these electrons acquires high energies by interacting with plasma waves, decreasing the conversion efficiency and producing harmful ( $\hbar\omega > 0.1$ –1 MeV) radiation. The production of electrons with energy much greater than that of the quiver motion is determined by the interaction time of an electron with the plasma waves. The use of a short laser pulse with duration comparable to the time of the plasma wave amplification can considerably reduce the population of energetic electrons; their temperature remains very high, which contributes to efficient  $K\alpha$  emission. The study of electron energy distribution in plasmas irradiated by short laser pulses is desirable to improve the characteristics of x-ray sources.

A short laser pulse is inevitably accompanied by a long prepulse of amplified spontaneous emission (ASE) [9]. ASE pulses have typically a pulse duration of 0.5–8 ns and a contrast ratio of  $10^{-7}$ – $10^{-6}$ . Even for a short laser pulse at moderate intensity ( $\sim 10^{17}$  W/cm<sup>2</sup>), the ASE pulse creates a plasma corona. The interaction of the main part of the short laser pulse with this plasma corona can change its absorption rate and hot electron distribution, resulting in x-ray spectra from the target surface. Since this interaction is sensitive to

the plasma density gradient, the prepulse effect becomes important with increasing laser intensity.

In the present paper we study the energy distribution of hot electrons produced by a short, 42 fs, laser pulse of moderate intensity  $\sim 10^{17}$  W/cm<sup>2</sup>,  $\lambda = 780$  nm, and the consequent  $K\alpha$  emission of a Cu slab target via direct spectroscopic measurements of x rays and a hybrid simulation which includes a hydrodynamic model, a collisional particle-in-cell (PIC) model with transient plasma ionization, and a Monte Carlo electron transport model. We show numerically in the distribution of hot electrons a clear energy cutoff at about  $2T_h$ , where  $T_h$  is the temperature of hot electrons. The energy cutoff reflects the fact that hot electron randomization cannot be completed during the short time of the laser-plasma interaction. The laser prepulse originating from ASE affects the character of the laser-plasma interaction. We find strong coupling between the incoming and outgoing parts of the laser pulse near the critical density in the plasma corona. This coupling leads to a high absorption rate and dominates the distribution of hot electrons. The energy cutoff is observed as a cutoff in the x-ray spectrum in our direct spectroscopic measurement. The results of our measurements and calculation agree well in both the soft (2–10 keV) and hard (20–40 keV) x-ray regions of the spectrum.

### II. EXPERIMENT

The scheme of the experiment is shown in Fig. 1. A table top terawatt laser system [7], which consists of a Ti-sapphire laser (Coherent Mira 900) and a chirped pulse amplification system, operating at 10 Hz is used to initiate x-ray emission from a Cu disk (with 70 mm diameter and 5 mm thickness) with a polished surface. The oscillator is a Kerr effect mode-

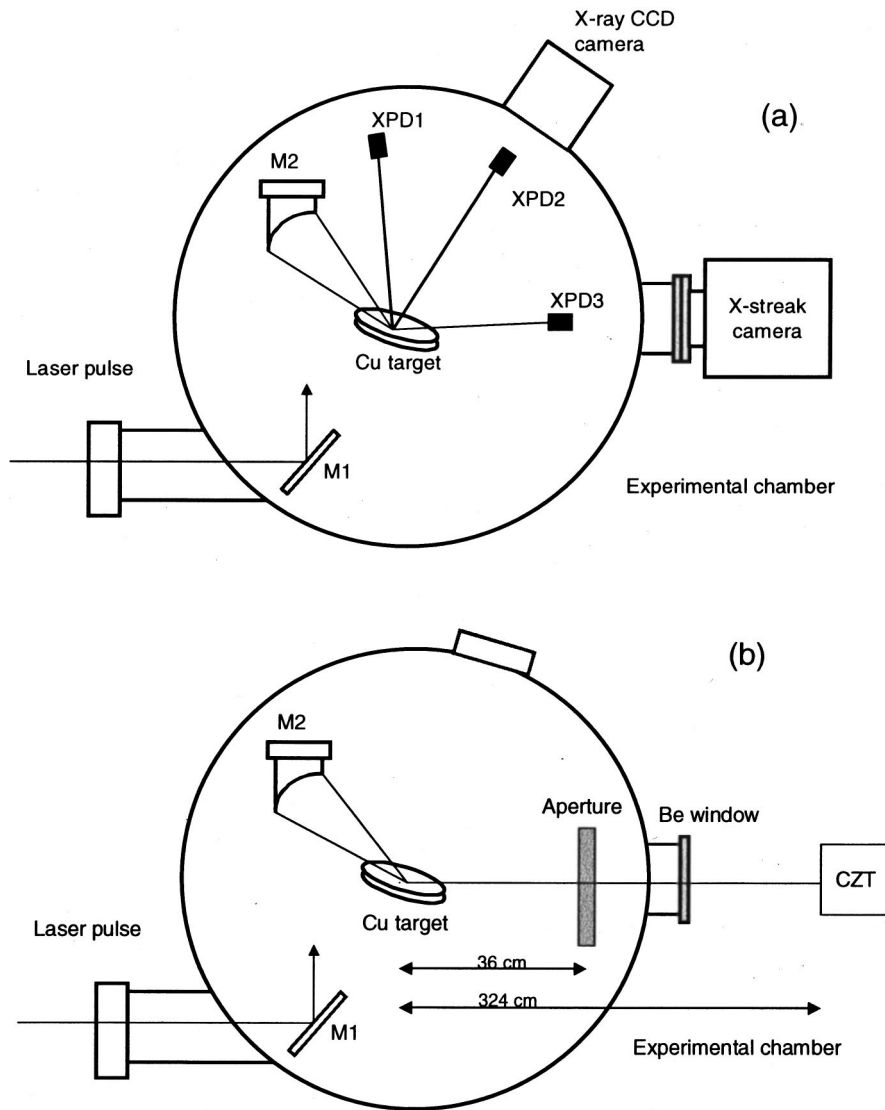


FIG. 1. The scheme of the experimental setup (a) for the x-ray streak and CCD cameras, and (b) for the CZT detector.

locking type Ti-sapphire laser that generates pulses of 25 fs at 76 MHz with an energy of 4 nJ. The bandwidth of the pulse is 35 nm [full width at half maximum (FWHM)] at 780 nm. The amplified laser beam has a pulse width of 300 ps, diameter of 50 mm, and maximum pulse energy of 400 mJ at wavelength  $\lambda = 785$  nm. The laser beam is guided into a vacuum chamber ( $10^{-6}$  Torr) and compressed to a pulse with duration of 42 fs. The contrast ratio between the main pulse and the prepulse that precedes it by 8 ns is greater than  $10^6:1$ . The amplified spontaneous emission appears 4 ns before the main pulse with a contrast ratio of  $10^6:1$ . A compressed laser pulse with an incident angle of  $57.5^\circ$  is focused on the target with a focal spot of  $44 \mu\text{m}$  in diameter by a parabolic mirror with a focal length of 165.2 mm and diameter of 76.2 mm. The laser intensity is estimated to be about  $10^{17} \text{ W/cm}^2$ .

The x-ray spectra with energy below 30 keV are measured with a direct-detection x-ray charge-coupled device camera (XCCD; Hamamatsu Photonics,  $512 \times 512$  pixels in a square of  $12 \times 12 \mu\text{m}^2$ ), which can analyze the positions and energy of the radiation in a photon counting mode. The XCCD temperature is maintained at  $-100^\circ\text{C}$  with liquid nitrogen. The XCCD system has an energy resolution of about

120 eV (FWHM) at 5.9 keV for single-pixel events. The XCCD chip has a  $500 \mu\text{m}$  thick beryllium window and is sensitive to x rays with energy over 2 keV. The XCCD is set 730 mm away from the focal spot. The integrated intensity of the x rays is also measured with an x-ray silicon photodiode (XPD; International Radiation Detector, AXUV-20HE1). The XPD is sensitive to x rays with energy between 4 and 30 keV. Three XPD's are set at a distance of 265 mm from the laser focal spot at different angles,  $0^\circ$ ,  $42^\circ$ , and  $65^\circ$  to the target surface normal.

The higher-energy x rays ( $<100$  keV) are measured with another technique. The x rays emerge from the chamber through a beryllium foil with  $100 \mu\text{m}$  thickness, and then are detected with a semiconductor detector (CZT,  $\text{Cd}_{0.9}\text{Zn}_{0.1}\text{Te}$ ; Amptek Inc., XR-100T-CZT). The detector is sensitive to x rays with energy from 5 V to 100 keV with an efficiency of almost 100%. The calibration of energy is performed using a standard  $\gamma$ -ray source ( $^{241}\text{Am}$ ). The detector is located 324 cm from the x-ray source. An aperture is used near the source to collimate its x-ray beam and to achieve the single-photon event. In the present experiments the single-photon counting condition of the CZT is checked only by the photon counts, which should be lower than 10 counts per second

because of the laser repetition rate (10 Hz). The aperture is a 1 mm pinhole in a 22 mm thick lead wall and is set 36 cm from the plasma. The energy resolution of the detector is estimated to be about 0.6 keV per point in the present experimental conditions. A total x-ray intensity between 4 and 30 keV is also measured by XPD.

### III. SIMULATION TECHNIQUE

We divide the calculation of the x-ray emission into three steps, the hydrodynamics of the ablated plasma expansion, the energy spectrum of hot electrons, and the x-ray emission process. The first is the calculation of the dynamics of the plasma corona. Because the intensity of the long pulse radiation of the amplified spontaneous emission is small, typically  $10^{11}$ – $10^{12}$  W/cm<sup>2</sup>, parameters of the plasma corona may be evaluated in the framework of a hydrodynamics model. In the second step, these parameters are used as an initial condition for the calculation of the interaction of the plasma with the main laser pulse. This modeling uses the particle-in-cell method to calculate the hot electron distribution function. Finally, the sampled electron distribution is used in the Monte Carlo calculation of  $K\alpha$  and Bremsstrahlung x-ray spectra.

#### A. Plasma hydrodynamics

We apply the HYADES code [10] to calculate parameters of the plasma corona produced by the amplified spontaneous emission. HYADES is a one-dimensional, one-fluid, three-temperature, radiation hydrodynamics simulation code. The code solves the equations of mass and energy transport in a Lagrangian coordinate system. Each fluid component is assumed to be in local thermodynamic equilibrium (LTE) with its own temperature. Electrons and ions are described by classical statistics, and radiation is approximately Planckian. The flux-limited diffusion approximation models transport phenomena. Radiation flux is calculated in a frequency averaged flux-limited approximation. The degree of ionization is described by the Saha model, or by the Thomas-Fermi model, or by the screened hydrogenlike average-atom model. Thermodynamic quantities are derived either from the ideal gas model or from an equation of state table. Electron degeneracy effects are included in the transport coefficients where appropriate. In the present calculation for a Cu target, we use the average ion model with the equation of state QEOS [11]. The external source of energy is the time-dependent laser field. The contrast ratio is chosen to be  $10^6:1$ , and the prepulse duration is 4 ns. The 10  $\mu\text{m}$  Cu target is approximated by a plane geometry with a nonuniform grid with 500 cells.

#### B. Electron energy spectrum by collisional PIC simulation with plasma ionization

We employ a hybrid PIC simulation [12], one dimensional in space and three dimensional in velocity space, which incorporates nonlocal thermodynamic equilibrium (non-LTE) ionization and adopts the Langevin equation to account for elastic collisions to compute the interaction of the plasma with the main laser pulse. In the Maxwell equations, we modify the Bourdier boost reference technique [13], for both  $p$ - and  $s$ -polarized laser pulses, to account for

the absorption of obliquely incident laser light. We get the following equation for the laser fields:

$$\frac{\partial}{\partial x} A_{\pm} \pm \sin \theta \frac{\partial}{\partial \tau} A_{\pm} = -\frac{1}{2} j_Y \sin \theta \mp \frac{1}{2} \cos \theta \left( j_X + \frac{\partial E_{ST,X}}{\partial \tau} \right),$$

$$H_Z = (A_+ + A_-) / \sin \theta, \quad E_{L,Y} = A_+ - A_-,$$

$$E_{L,X} = (A_+ + A_-) \cos \theta / \sin \theta \quad (1)$$

for the  $p$ -polarized pulse and

$$\frac{\partial}{\partial x} A_{\pm} \pm \sin \theta \frac{\partial}{\partial \tau} A_{\pm} = -\frac{1}{2} j_Z,$$

$$H_Z = A_+ - A_-, \quad E_{L,Z} = (A_+ + A_-) / \sin \theta,$$

$$H_X = -(A_+ + A_-) \cos \theta / \sin \theta \quad (2)$$

for the  $s$ -polarized pulse, where  $E$  and  $H$  are the electric and magnetic fields,  $j$  is the current and  $\theta$  is the angle of incidence.

We introduce a kinetics grid [12,14,15] to determine the plasma parameters. With the scale length of the change of the electron density mainly determined by the electron mean free path rather than the Debye length, approximately 20 PIC cells are combined to form a kinetics cell. It also provides statistics for the calculation of the temperature, density, and fluid velocity. Plasma ionization and its temporal evolution are considered by calculating the charge of computational particles (CPs). Simple atomic kinetics based on the average-ion model [12], in which the ionization potential  $I_z$  is a function of ion charge  $z$ , is used to calculate the charge, namely, the change of plasma electrons is calculated by an electron balance equation that includes electron collisional ionization and field ionization in the presence of intense laser light. We use the field ionization probability  $\tau^{-1}$  (see Ref. [16]) with the electric field strength  $E_k$  averaged over the  $k$ th cell. Using the electron balance equation we compute the charge change  $\Delta Q_{ek}$  in every kinetic cell. Then, electrons acquire the charge  $\Delta Q_{ek}/N_{ek}$  and ions  $\Delta Q_{ek}/N_{ik}$ , where  $N_{ek}$  and  $N_{ik}$  are the numbers of particles in the  $k$ th cell. While the electron charge-to-mass ratio is kept constant, the ion's increases with  $z$ . To compensate for the energy loss due to optical field ionization (OFI)  $W_{\text{OFI}}$ , we include an effective atomic current in the Maxwellian equation  $\mathbf{j}_A(t)\mathbf{E}_L(t-\Delta t) = W_{\text{OFI}}(t-\Delta t)$ , with  $\mathbf{E}_L$  being the laser electric field. The energy loss due to collisional ionization is calculated as an effective friction. This model has been checked via the kinetic simulation of laser-irradiated carbon and silicon overdense plasmas [12].

The results of the hydrodynamics calculation are employed as the initial condition. For that, the temperature, density, and average ion charge are approximated on the kinetic grid. Only 0.5  $\mu\text{m}$  of the solid target is included, while the size of the plasma corona is varied from 1 to 20  $\mu\text{m}$ . CPs are redistributed in accordance with those approximations. The typical number of particles is  $3 \times 10^5$  per species.

### C. X-ray spectrum by Monte Carlo transport code

We utilize the time-independent, coupled electron-photon Monte Carlo codes of the TIGER series (ITS) [17,18] to simulate interaction of hot electrons with the solid target. These codes use an elaborate ionization/relaxation model including  $K$ ,  $L1$ ,  $L2$ ,  $L3$ ,  $M$ , and  $N$  shells to treat the range of 1–10 keV x rays. In the present work, we use the ACCEPTP code, which is valid for problems with axial symmetry, without magnetic and electric fields, with appropriate resolution in the 1 keV to 1 MeV range of the x-ray spectrum. While the targets and incident electron beam specified in the code must have axial symmetry, the electron trajectories are three dimensional. The code tracks the electrons in the initial beam as well as all secondary electrons produced during interaction with the target and calculates the production of characteristic radiation in addition to Bremsstrahlung radiation. Since the results are the output of a single electron with a fixed energy, the number of  $K\alpha$  photons and x-ray spectra are further calculated by averaging the sampled distribution from the PIC simulation.

## IV. RESULTS AND DISCUSSION

### A. $K\alpha$ emission of a Cu slab

The efficiency of  $K\alpha$  emission from the target surface per electron may be approximately estimated for the energy of the electron by neglecting elastic scattering and using the Bethe formula [19],

$$\eta \approx \frac{A_Z}{A_Z + \Gamma_Z} \sum_{\varepsilon - kE_Z^1 > 0} \frac{\ln[(\varepsilon - kE_Z^1)/E_Z^1]}{\sum_n \ln[(\varepsilon - kE_Z^1)/E_Z^n]} \times \exp\left(-\frac{\sigma_{\text{phot}}(\hbar\omega)}{\sigma_Z(\varepsilon/E_Z^1)}\right), \quad (3)$$

where  $\varepsilon$  is the energy of the electron in keV,  $E_Z^n$  is the ionization energy from the  $n$  shell,  $A_Z \sim (4.8 \times 10^8) Z^4 \text{ s}^{-1}$  is the radiation probability,  $\Gamma_Z \sim 10^{15} \text{ s}^{-1}$  is the autoionization rate, and  $\sigma_{\text{phot}}$  is the photoionization cross section and  $\sigma_Z$  the collisional ionization cross section. The first multiplier in Eq. (3) determines the probability of radiative transition, the second one is the probability of inner-shell ionization, the third one describes x-ray absorption due to photoionization in the ( $n=2$ ) shell by a  $K\alpha$  photon at the distance  $l \sim 1/(\sigma_i N)$ , where  $\sigma_i$  is the collisional ionization cross section of the inner shell. Numerically, the exponent is close to the ratio

$$\frac{\sigma_{\text{phot}}(\hbar\omega)}{\sigma_Z(\varepsilon/E_Z^1)} \approx \frac{0.1\varepsilon}{\ln(\varepsilon/E_Z^1)}.$$

The sum in Eq. (3) weakly depends on the energy of electrons and may be estimated as  $\text{sum} = \alpha \text{int}(\varepsilon/E_Z^1)/Z$ , where  $Z$  is the nuclear charge and  $\alpha \sim 1$ . For a Cu target, the probability  $\eta$  does not exceed  $10^{-2}$  at any energy of electrons and decreases at high electron energies due to an increase of absorption with penetration depth. Figure 2(a) shows the dependence of the probability or of the number of  $K\alpha$  photons per electron,  $\eta$ , on the electron energy calculated by the ACCEPTP code. The probability reaches a maximum value at  $\varepsilon = 200$  keV. The total number of  $K\alpha$  photons depends on

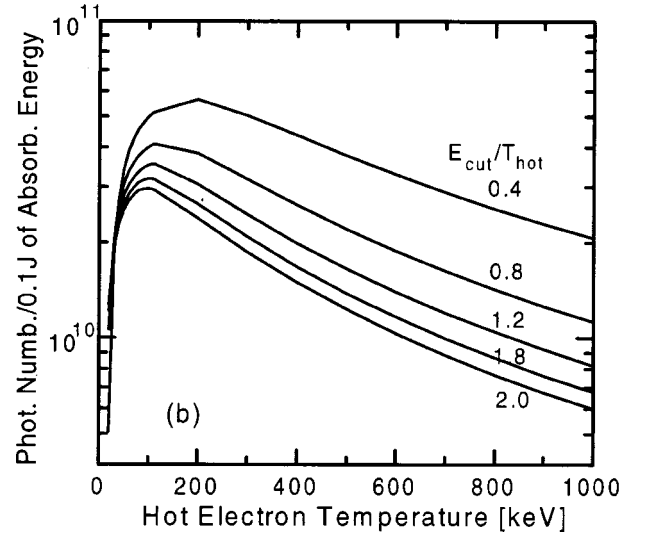
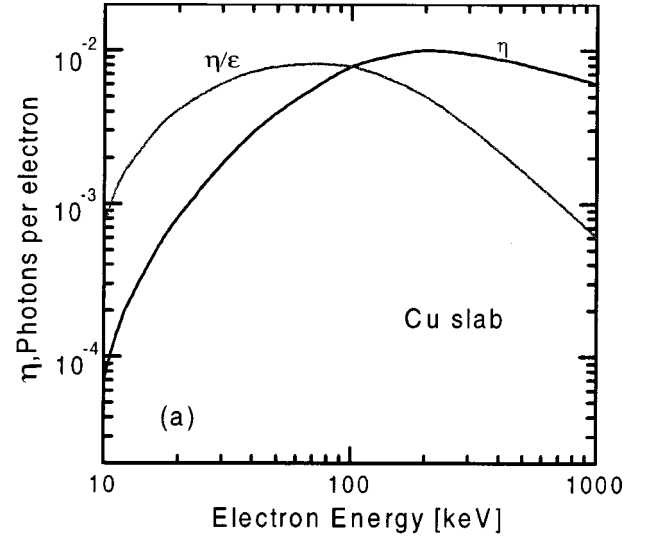


FIG. 2. The efficiency of backward  $K\alpha$  emission per electron from a Cu slab as a function of the energy of the electron (a) and the number of backward emitted  $K\alpha$  photons per 100 mJ of laser energy for different temperatures of hot electrons with the energy cutoff  $E_{\text{cut}}$  (b).

the number of hot electrons, which is proportional to  $W/\varepsilon$  with  $W$  the total laser energy, so that the value of  $\eta/\varepsilon$  is a more accurate characteristic for that total photon number. This value,  $\eta/\varepsilon$ , reaches a maximum at a considerably lower energy,  $\varepsilon = 50$ – $60$  keV. It depends slightly on the energy from 20 to 200 keV and rapidly decreases beyond 200 keV. The electron energy also dominates the duration of  $K\alpha$  emission. This time is approximately equal to the time of inner-shell ionization. Using the Lotz formula

$$\sigma_Z \approx (4 \times 10^{-14}) \xi \frac{\ln(\varepsilon/E_Z)}{\varepsilon E_Z} \text{ cm}^2, \quad (4)$$

for the ionization cross section (energy is given in eV), where  $E_Z$  is the ionization energy and  $\xi$  is the number of equivalent electrons in a shell, and using the ion density of a Cu target, one obtains the mean inner-shell ionization time of  $t = (\sigma_Z \nu N_{\text{Cu}})^{-1} = 7.2 \text{ ps} [(\varepsilon/20 \text{ keV})^{1/2}]$ .

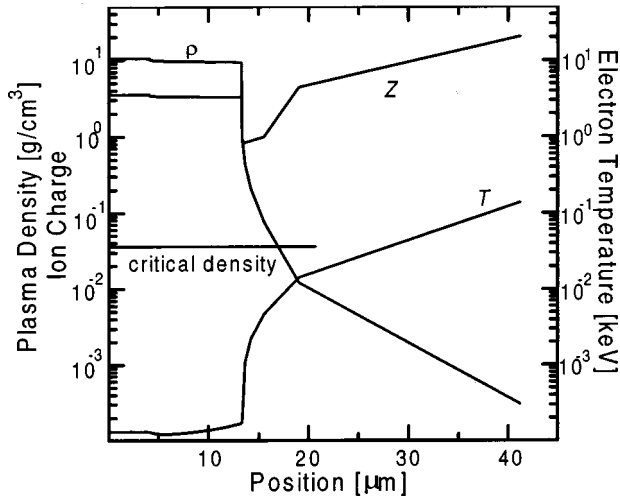


FIG. 3. The parameters of the Cu plasma produced by the laser prepulse with the contrast ratio  $10^6:1$  and duration of 4 ns.

To estimate the number of  $K\alpha$  photons for a comparably long laser pulse, one may adopt a Maxwellian distribution for hot electrons [20,21]. Because the dependence of  $\eta$  on the electron energy up to  $\varepsilon=200$  keV is approximately linear, the total number of  $K\alpha$  photons, which are irradiated backward, is

$$N_{K\alpha} = \eta(T_h) \frac{\nu W}{\chi T_h},$$

where  $T_h$  is the temperature of hot electrons,  $\nu$  is the laser absorption efficiency, and the coefficient  $\chi$  varies from 0.5 for an anisotropic distribution to 1.5 for an isotropic one.  $N_{K\alpha}$  depends mainly on the laser energy. In the case of very short laser pulses, the distribution can have an energy cutoff. The energy cutoff, as seen in Fig. 2(b), leads to an increase in the  $K\alpha$  output.

### B. Absorption of the short laser pulse

Shown in Fig. 3 are the calculated parameters of the plasma corona after a 4 ns ASE pulse with intensity  $I = 10^{11}$  W/cm<sup>2</sup>. The maximal ion charge is approximately  $z = 15$ , while the plasma temperature exceeds 100 eV. The density profile has a complex form and cannot be approximated by a single exponent. The density gradient is approximately  $L/\lambda = 2.5$  in the vicinity of the critical density, much greater than the optimal density gradient for resonance absorption,  $L/\lambda \sim 0.1-0.2$  [12,22]. Following the results of Ref. [22], one would expect a very low absorption rate in this region of the density gradient.

The temporal evolution of the absorption rate of the short laser pulse with intensity of  $10^{17}$  W/cm<sup>2</sup> is given in Fig. 4. The absorption rate displays strongly nonlinear behavior under these conditions. The maximal absorption rate can exceed 60% at the time when the strong coupling of the incoming and outgoing (reflected) parts of the laser field with the plasma arises near the critical density. This happens when the outgoing part of the pulse completely overlaps with the rest of the incoming part. When the pulse passes through, only its reflected part is involved in the absorption process, so that the final absorption efficiency is only 25%. When the

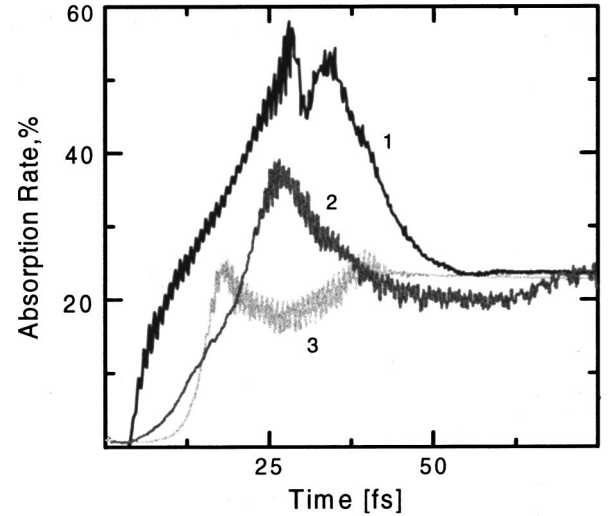


FIG. 4. The temporal evolution of the absorption rate of a  $p$ -polarized laser pulse,  $\lambda = 780$  nm, with intensity  $I = 10^{17}$  W/cm<sup>2</sup> and 42 fs duration. (1) Gaussian shape pulse, (2) sinelike shape pulse,  $L/\lambda = 2.5$ , (3) Gaussian pulse,  $L/\lambda = 1.25$ .

laser pulse is nonmonochromatic, the maximal absorption rate can be 80% for  $p$  polarization. The interaction is also sensitive to the pulse shape. We believe that the hot electron distribution is formed mainly at the time of strongest laser-plasma interaction, when the self-overlapping occurs. With a shorter prepulse, 2 ns, and the same contrast ratio, which corresponds to the density gradient  $L/\lambda \sim 1$ , the resonance interaction disappears, though the total absorption rate does not change. The absorption rate exhibits a nonlinear interaction for an  $s$ -polarized pulse as well. The maximal absorption rate is about 40% in this case.

### C. X-ray emission and electron energy cutoff

In Fig. 5 we present the results of measurements and calculation of the spectrum in a soft part of the plasma x-rays. The results of the ACCEPTP calculation of x-ray emission including  $K\alpha$  from the Cu target irradiated by a monochromatic  $e$  beam (an electron with given energy) with different energies are given in Fig. 5(a). The ratio of Bremsstrahlung radiation at 2–4 keV energy and  $K\alpha$  emission is sensitive to the energy of electrons so that we expect a strong dependence of this ratio on the electron energy cutoff and hot electron temperature. The sampled distribution of plasma electrons in the plasma irradiated by  $s$ - or  $p$ -polarized laser pulses is shown in Fig. 5(b). An energy cutoff is clearly seen in the figure. We define the energy cutoff as the energy at which the density of hot electrons is much smaller than Maxwellian-like with  $T_h$ . In the case of the  $p$ -polarized pulse the energy cutoff is about 30 keV, while for the  $s$ -polarized pulse it is only 20 keV. Although the temperature of hot electrons in keV is close to the approximation [20,21]

$$T_h = 30 [I \lambda^2 / 10^{17} (\text{W } \mu\text{m}^2 / \text{cm}^2)]^{1/3} [T_c \text{ keV}]^{1/3}$$

with  $T_c$  the temperature of the background plasma, the duration of the laser pulse is too short to allow the complete randomization in energies of hot electrons. In the case of the  $p$ -polarized laser pulse, we observe a small fraction of ener-

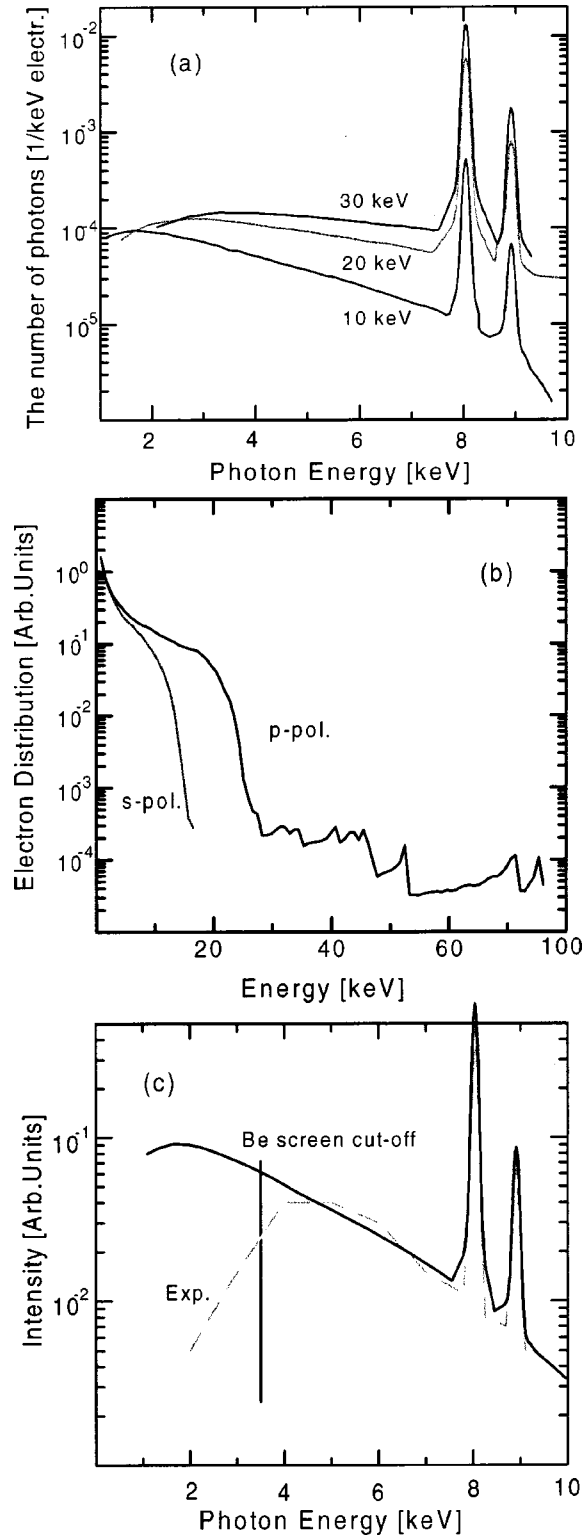


FIG. 5. The hot electron distribution and soft x-ray spectrum of a Cu plasma irradiated with a 42 fs laser pulse with an energy of 50 mJ. The number of x-ray photons emitted from a Cu target irradiated with an electron at different energies (a); the electron distribution produced by the laser pulse with *s*- and *p*-polarization (b); the measured (dashed line) and calculated with sampled distribution (solid line) spectra of x-ray emission from the Cu plasma (c); the vertical line shows the limit of transparency of the Be screen.

getic electrons forming a tail up to 100 keV. The effective temperature of electrons in the tail is considerably higher than  $T_h$ . The soft x-ray spectrum [7] from 2 to 10 keV is shown in Fig. 5(c). A good agreement between the calculation made with the sampled electron distribution and the measurement occurs not only for the intensity ratio, but also for the slope of the Bremsstrahlung radiation. The discrepancy in the region below 3.5 keV is attributed to absorption by a Be shield which is used to protect the detector.

To demonstrate the existence of the energy cutoff, we make a comparison for hard x rays from 20 to 40 keV. In Fig. 6(a) we present the results of the calculation for the x-ray spectrum produced by monoenergetic electrons. We use these results to evaluate the spectrum by weighting them with the electron distribution obtained from the PIC simulation with the experimental conditions [see Fig. 6(b)]. The comparison given in Fig. 6(c) shows good agreement. An electron energy cutoff at 40 keV is noticed. We further note that the results of the calculation agree better with the experimental ones for the *p*-polarized pulse. The calculated and measured dependences of the  $K\alpha$  emission output on the laser energy are shown in Fig. 7. The results are close for laser energies over 30 mJ. With the laser energy changing only by a factor of 3, the energy of the  $K\alpha$  output increases by two orders of magnitude, displaying the effect of the energy cutoff.

The dependence of reflectivity and energy cutoff on the density gradient in the vicinity of the critical density, in other words on the ASE pulse energy, is presented in Fig. 8. For a low density gradient,  $L/\lambda \sim 0.1-0.2$ , which is optimal for resonance absorption, the absorption efficiency is high, over 50%, and the electron energy cutoff is about 200 keV. These results are similar to those from the measurement [22] made for a Si plasma. With an increase in density gradient, the absorption efficiency decreases until a resonance interaction of the incoming and outgoing pulses with the plasma appears. The electron energy cutoff in the plasma with a large density gradient, about 40 keV, is much smaller. According to the calculation, we find that the total number of  $K\alpha$  photons is the same as in the case of small and large density gradients in spite of the lower absorption rate. This is again because of the energy cutoff.

#### D. Laser pulse of relativistic intensity

We believe that the electron energy cutoff appears even in the case of a laser pulse with relativistic intensity  $I\lambda^2 > 10^{18} \text{ W}\mu\text{m}^2/\text{cm}^2$ . However, the resonant relativistic processes of laser-plasma interaction can drastically decrease the time for randomizing which would lead to a very high maximal energy for hot electrons. To show this, we consider the interaction of an *s*-polarized laser pulse (100 TW, 20 fs [23]) with a plasma with a small density gradient. Existence of the relativistic resonance (see also [24]) can be shown via the following estimation. The electron motion in the electromagnetic plane wave,

$$E_Y = A \cos(\omega t + kx), \quad H_Z = -A \cos(\omega t + kx),$$

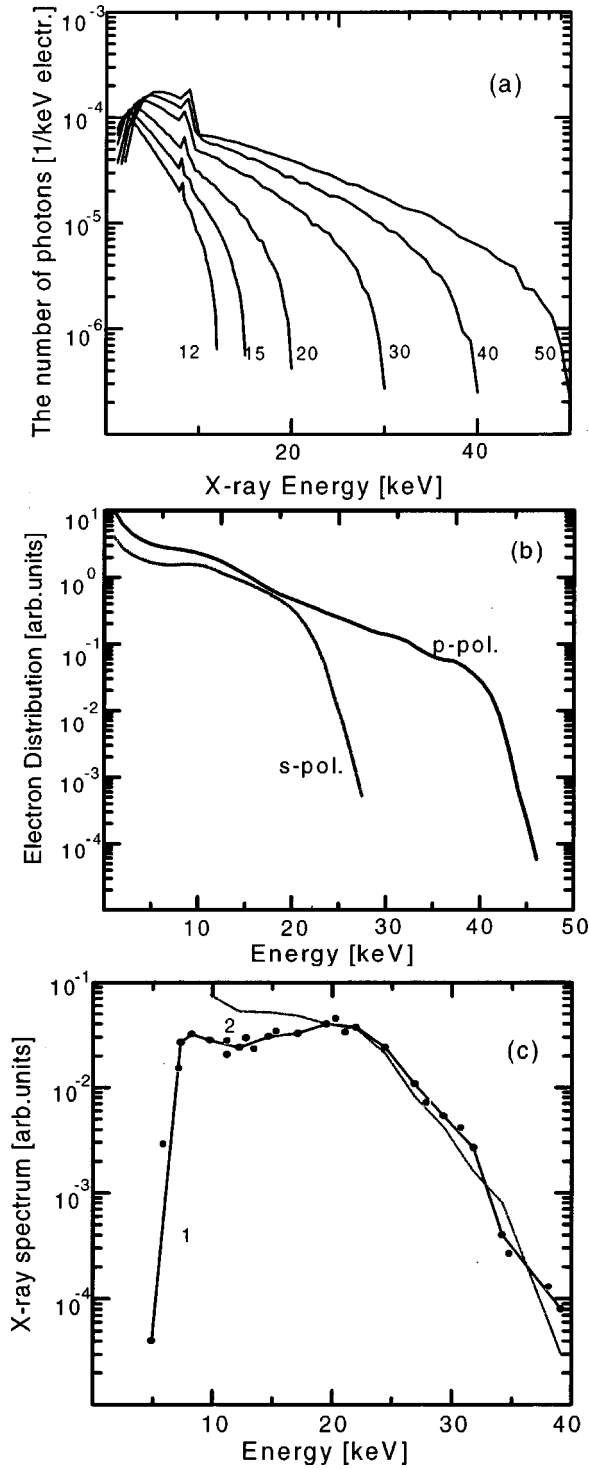


FIG. 6. The hot electron distribution and hard x-ray spectrum of a Cu plasma irradiated with a 42 fs laser pulse with an energy of 90 mJ. The number of x-ray photons emitted from a Cu target irradiated with an electron at different energies (a); the electron distribution produced by the laser pulse with *s*- and *p*-polarization (b); the measured (line with dots) and calculated (solid line) spectra of x-ray emission from the Cu plasma (c).

can be found in the laboratory reference frame. Assuming a force due to the plasma electrostatic field of the form  $F_x = -m\omega_{\text{pl}}^2 x$ , where  $x$  is the electron coordinate and  $\omega_{\text{pl}}$  the plasma frequency, one finds

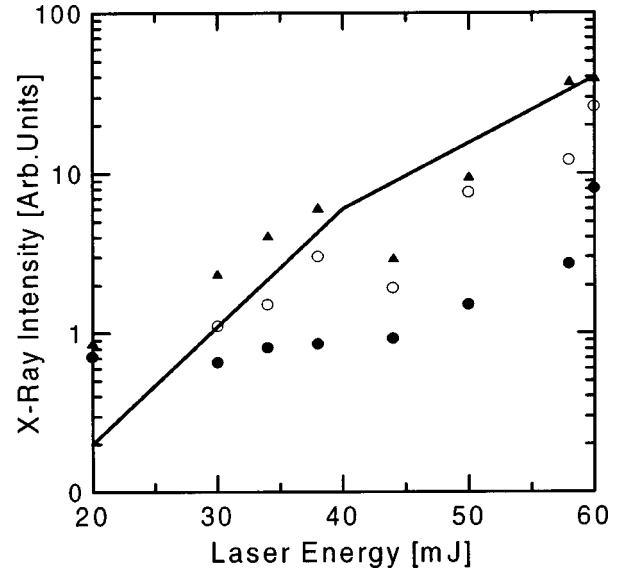


FIG. 7. Dependence of Cu *K*α output on the energy of the laser pulse; the calculated total (solid line) and measured output in the direction at 25° to the plasma surface (solid triangles), 48° (open circles), and 0° (solid circles).

$$u_y = -\tilde{A} \sin(\tau + \tilde{x}) + u_y^0,$$

$$\dot{u}_x = -\alpha^2 \tilde{x} - \frac{1}{2} \tilde{A}^2 \sin(2\tau + 2\tilde{x}) / \gamma + u_y^0 \cos(\tau + \tilde{x}) / \gamma,$$

$$\gamma = \sqrt{1 + u_x^2 + [u_y^0 - \tilde{A} \sin(\tau + \tilde{x})]^2},$$

$$\tilde{x} = u_x / \gamma, \quad (5)$$

with  $\tilde{A} = eA/mc\omega$ ,  $\mathbf{p} = mc\mathbf{u}$ ,  $\tau = \omega t$ ,  $\tilde{x} = \omega x/c$ , and  $\alpha = \omega_{\text{pl}}/\omega$ ,  $A$  is the amplitude of the electromagnetic wave and  $u^0$  the initial momentum of the electron. The  $x$  component of the momentum can be expressed in the form of an implicit equation

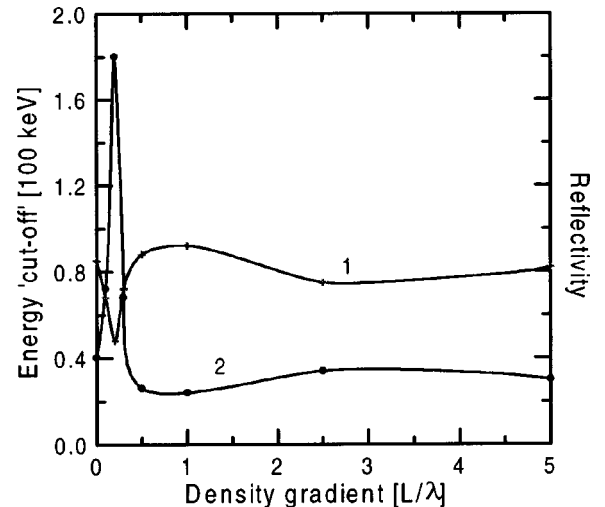


FIG. 8. The dependence of the reflectivity (1) and the electron energy cutoff (2) on the density gradient in the vicinity of the critical density for a (90 mJ) 42 fs laser pulse.

$$u_x = \frac{1 + u_Y^2 - (\gamma_0 + u_X^0 - \alpha^2[\bar{x}^2/2 + \int \bar{x} d\tau])^2}{2(\gamma_0 + u_X^0 - \alpha^2[\bar{x}^2/2 + \int \bar{x} d\tau])} \quad (6)$$

with  $\gamma_0 = \gamma(t=0)$  determined by the initial velocity of the electron. According to Eq. (6) the resonance condition appears at  $\omega_{\text{pl}} = 2\omega$  if  $A \sim 1$ . With an increase of the wave amplitude, the resonance condition shifts toward  $\omega_{\text{pl}} = \omega$ . At very high laser intensity, a set of resonances covers the interval  $[\omega, 2\omega]$ . These conditions determine the optimal density gradient, which must increase with the laser amplitude  $A$ .

The results of the simulation of the interaction of a 20 fs laser pulse with the Cu slab target are shown in Fig. 9. At a low intensity, we observe no resonance interaction in the small density gradient scale region  $L \sim (0.1-0.3)\lambda$ . The resonance interaction appears at a laser intensity of  $I\lambda^2 > 2 \times 10^{18} \text{ W } \mu\text{m}^2/\text{cm}^2$ . Initially, the absorption efficiency is maximal at the density gradient corresponding to the resonance at  $2\omega$  while, with the laser intensity, the density gradient increases to that determined by the resonance condition at  $\omega_{\text{pl}} = \omega$ . The temporal evolution of the electron distribution function is presented in Fig. 9(b). Without the resonance condition the energy cutoff of hot electrons is quite low, about 200 keV. Due to the resonance condition the temperature of hot electrons at the optimal density gradient increases considerably and can exceed 1 MeV with the energy cutoff exceeding 5–10 MeV.

## V. CONCLUSION

We have found a clear energy cutoff in the distribution of hot electrons produced during the interaction of a short laser pulse of moderate intensity with solid targets. This energy cutoff is about  $2T_h$  and strongly depends on the contrast ratio of the ASE pulse and the main laser pulse. A hydrodynamic calculation shows that for a typical contrast ratio the plasma corona formed by the ASE pulse can have a large density gradient  $L/\lambda \sim 1-2$  even for a moderate intensity laser pulse. This results in the interaction of the plasma with the main laser pulse. We showed via PIC simulation that, due to the effective coupling of the plasma with both the incoming and the outgoing (reflected) laser pulses in the vicinity of the critical density, the maximal absorption rate exceeds 60%, while the overall absorption efficiency is about 25%. The most energetic hot electrons are produced at the time of the intense interaction of the plasma with both laser pulses. This interaction also depends on the incoming pulse shape. We demonstrated through Monte Carlo simulation that the  $K\alpha$  output is more efficient with a hot electron energy cutoff and has a shorter pulse duration. For a laser intensity of  $10^{17} \text{ W/cm}^2$  and pulse duration about 40 fs, the  $K\alpha$  emission efficiency is about  $(1-2) \times 10^{-4}$  and the pulse duration is shorter than 7 ps. The x-ray properties, i.e., the small energy cutoff  $E_{\text{cut}} < 100 \text{ keV}$ , the high efficiency, and

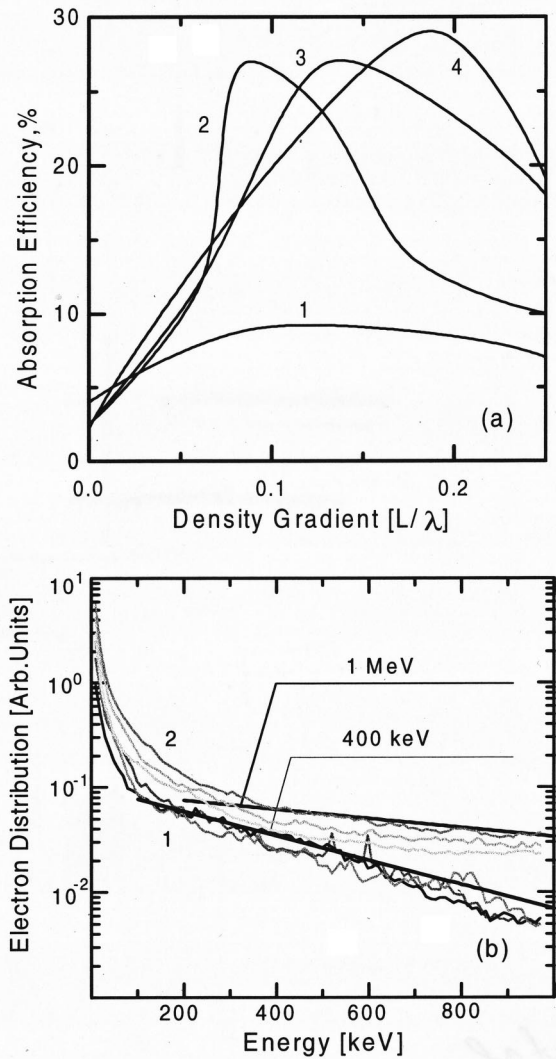


FIG. 9. The absorption efficiency (a) and hot electron distribution (b) for a 20 fs laser pulse of relativistic intensity and  $s$ -polarization at different density gradients. The laser intensity is (a) (1)  $4 \times 10^{18}$ , (2)  $10^{19}$ , (3)  $4 \times 10^{19}$ , (4)  $10^{20} \text{ W/cm}^2$ ; (b) (1)  $10^{19}$ ,  $L/\lambda = 0.1$  (2)  $10^{20} \text{ W/cm}^2$ ,  $L/\lambda = 0.2$ .

the short pulse duration of Cu  $K\alpha$  emission at 8 keV make such a table-top laser x-ray source safe and practical in various applications.

## ACKNOWLEDGMENTS

The experimental work was supported by the Core Research for Evolutional Science and Technology (CREST) project of Japan Science and Technology Corporation. T.T. is supported by U.S. DOE Contract No. W-7405-Eng-48. We also thank Dr. K. Yamakawa and Dr. J. Koga at the Japan Atomic Energy Research Institute for valuable discussions.

- [1] J. A. Cobble, G. T. Schappert, L. A. Jones, A. J. Taylor, G. A. Kyrala, and R. D. Fulton, *J. Appl. Phys.* **69**, 3369 (1991).  
 [2] A. Rouse, P. Audebert, J. P. Geindre, F. Fallies, J. C. Gauthier, A. Mysyrowicz, G. Grillon, and A. Antonetti, *Phys. Rev. E* **50**,

2200 (1994).

- [3] T. Feurer, W. Theobald, R. Sauerbrey, I. Uschmann, D. Altenberd, U. Teubner, P. Gibbon, E. Forster, G. Malka, and J. L. Miguel, *Phys. Rev. E* **56**, 4608 (1997).

- [4] F. N. Beg, A. R. Bell, A. E. Dangor, C. N. Danson, A. P. Fews, M. E. Glinsky, B. A. Hammel, P. Lee, P. A. Norreys, and M. Tatarakis, *Phys. Plasmas* **4**, 447 (1997).
- [5] J. Yu, Z. Jiang, and J. C. Kieffer, *Phys. Plasmas* **6**, 1318 (1999).
- [6] T. Guo, C. Rose-Petruck, R. Jimenez, F. Raksi, J. Squier, B. Walker, K. R. Wilson, and C. P. J. Barty, *Proc. SPIE* **84**, 3157 (1997).
- [7] M. Yoshida, Y. Fujimoto, Y. Hironaka, K. G. Nakamura, K. Kondo, M. Otani, and H. Tsunemi, *Appl. Phys. Lett.* **73**, 2393 (1998).
- [8] D. C. Eder, G. Pretzler, E. Fill, K. Eidmann, and A. Saemann, *Appl. Phys. B: Lasers Opt.* **70**, 211 (2000).
- [9] J. D. Kmetec, C. L. Gordon, J. J. Macklin, B. E. Lemoff, G. S. Brown, and S. E. Harris, *Phys. Rev. Lett.* **68**, 1527 (1992).
- [10] J. T. Larsen and S. M. Lane, *J. Quant. Spectrosc. Radiat. Transf.* **51**, 179 (1994).
- [11] R. M. More, K. H. Warren, D. A. Young, and G. B. Zimmerman, *Phys. Fluids* **31**, 3059 (1988).
- [12] A. Zhidkov and A. Sasaki, *Phys. Rev. E* **59**, 7085 (1999).
- [13] A. Zhidkov, A. Sasaki, T. Tajima, T. Auguste, P. D'Olivera, S. Hulin, P. Monot, A. Ya. Faenov, T. A. Pikuz, and I. Yu. Skobelev, *Phys. Rev. E* **60**, 3273 (1999).
- [14] P. Gibbon and A. R. Bell, *Phys. Rev. Lett.* **68**, 1535 (1992).
- [15] A. Zhidkov, A. Sasaki, and T. Tajima, *Phys. Rev. E* **61**, R2224 (2000).
- [16] A. Zhidkov and A. Sasaki, *Phys. Plasmas* **7**, 1341 (2000).
- [17] S. M. Seltzer, *Appl. Radiat. Isot.* **42**, 917 (1991).
- [18] M. J. Berger and S. M. Seltzer, National Bureau of Standards Report No. 9837, 1968 (unpublished).
- [19] L. V. Spencer and U. Fano, *Phys. Rev.* **93**, 1172 (1954).
- [20] D. W. Forslund, J. M. Kindel, and K. Lee, *Phys. Rev. Lett.* **39**, 284 (1977).
- [21] K. Estabrook and W. L. Kruer, *Phys. Rev. Lett.* **40**, 42 (1977).
- [22] S. Bastiany, A. Rousse, J. P. Geindre, P. Audebert, C. Quiox, G. Hamoniaux, A. Antonetti, and J. C. Gauthier, *Phys. Rev. E* **56**, 7179 (1997).
- [23] K. Yamakawa, JAERI Report No. Conf 2000-006, 2000 (unpublished), p. 29.
- [24] S. C. Wilks, W. L. Kruer, M. Tabak, and A. B. Langdon, *Phys. Rev. Lett.* **69**, 1383 (1992).